Available online at www.sciencedirect.com
SCIENCE DIRECT®
Journal of Power Sources 123 (2003) 163–171
JOURNAL OF POWER SOURCES
www.elsevier.com/locate/jpowsour

Further refinements in the segmented cell approach to diagnosing performance in polymer electrolyte fuel cells

Guido Bender*, Mahlon S. Wilson, Thomas A. Zawodzinski[1]

Electronic and Electrochemical Materials and Devices Group, MST-11, MS D429, Los Alamos National Laboratory, Los Alamos, NM 87545, USA

Received 6 March 2003; accepted 31 March 2003

Abstract

Described is the most recent configuration of a segmented cell used to measure current distribution across the surface of an electrode in a polymer electrolyte fuel cell (PEFC). In this fourth generation cell design, measurement and data collection capabilities have been modified to significantly improve ease of use and quality of information obtained. The current configuration allows examination of spatial resolution of the cell current and cell voltage with respect to well-defined baseline reference measurements, as well as measurement of the high frequency resistance (HFR) distribution and spatial ac impedance spectroscopy. This specially designed cell is intended for use in studies on time and location resolved carbon monoxide poisoning, humidification and flow-field design effects on fuel cell performance. Published by Elsevier B.V.

Keywords: PEMFC; PEFC; Design; Impedance; Current distribution; Segmented cell

1. Introduction

Polymer electrolyte fuel cells (PEFCs) are promising sources of electrical energy for stationary and transportation applications. However, to optimise PEFC performance a greater understanding of variations in current distribution in the fuel cell as a function of cell hardware design, operating conditions and component characteristics is required. One previously demonstrated approach to acquiring this information is through the use of a segmented fuel cell. The segmented cell is similar to an ordinary fuel cell with the exception that one of the electrodes is divided into several smaller electrodes each of which can be interrogated for current, voltage and resistance, independent of the other electrode elements. This configuration allows for mapping of the current distribution across the surface of the electrode.

The segmented cell for PEFCs was first introduced by Cleghorn et al. [1], who used a printed circuit board design to collect current distribution data. Use of this hardware contributed to an improved understanding of water management and reactant distribution over the active fuel cell electrode area. One problem associated with this early design was the necessity of using two electronic loads. There was no assurance that one did not influence the response of the other especially when there were large differences in potential between electrode segments. Another limitation was the time required to acquire information. Each electrode element had to be interrogated individually resulting in an experiment taking up to 12 h to obtain a single dataset in an 18-segment cell.

Subsequent improved segmented cell designs were offered by the German Aerospace Centre, Stuttgart [2] and Ballard Power Systems, Inc. [3] An evaluation of the advantages and disadvantages of each of these three systems has been provided by Stumper et al. [3] A similar analysis has led to the design of a LANL fourth generation segmented cell, which is described herein. This new design contains more sophisticated hardware and measurement capabilities that allows for measurement of current, voltage and high frequency resistance (HFR) from each electrode element simultaneously rather than sequentially, greatly reducing data acquisition time. The sensitivity of the measurements is also greatly enhanced over previous designs.

2. Experimental

2.1. Cell design and measurement setup

The segmented cell contained a one-piece cathode with an active surface area of 104 cm^2. The opposing anode had the same outer dimension but was divided into 10 segments each

* Corresponding author. Tel.: +1-505-667-1774; fax: +1-505-665-4292.
E-mail address: guido@lanl.gov (G. Bender).
[1] Present address: Case Western Reserve University, 10900 Euclid Avenue, Cleveland, OH 44106, USA.

0378-7753/$ – see front matter. Published by Elsevier B.V.
doi:10.1016/S0378-7753(03)00533-0

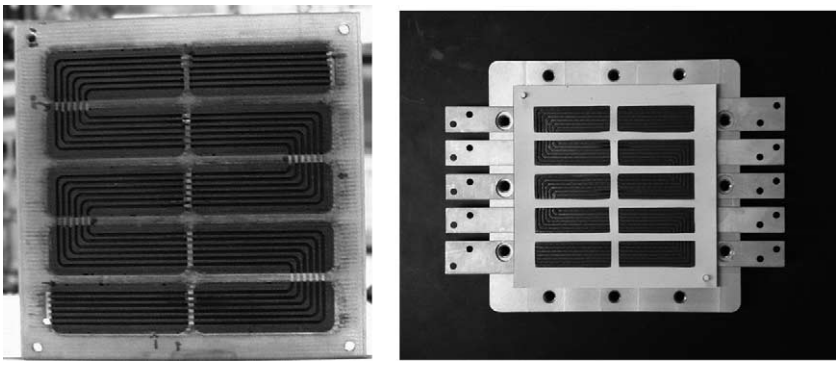

Fig. 1. Segmented anode flow-field consisting of graphite blocks embedded in Ultem® frame (left). Anode flow-field with endplate, current collector plates and gasket (right).

with 7.71 cm^2 active surface area identified as Seg01–Seg10 in this work. To prevent leakage of the fuel cell hardware and to improve the contact resistance of the single segments, this cell employed segments made of graphite blocks, which were inserted in an Ultem® (polyetherimide) frame using a two-component epoxy for sealing and attachment. Individual current collector plates for the segments, rather than wired contacts to the graphite blocks, allowed low contact resistance per segment and resulted in higher measurement accuracy. Fig. 1 shows the segmented flow-field, the current collector plates and the silicone rubber gasket of the anode. The anode catalyst layer, anode gas diffusion backing, and anode current collector were also segmented to match the anode hardware. The flow-field was six-fold serpentine channels feeding the fuel to the segments in consecutive order from gas inlet to gas outlet.

Fig. 2 shows a schematic of the segmented cell setup. The current lead wires of each segment were threaded through separate standard Hall sensor devices (BB-25, F.W. Bell). The bulk Hall sensors had a sensitivity of $V_{Hall} = 40\,mV/A$. Sensitivity of the device typically drifted with temperature $\pm 0.30\,mV/°C$. The offset voltage drifted up to $\pm 1.30\,mV/°C$. The Hall sensor devices were physically separated from the fuel cell hardware and housed in a constant temperature chamber to avoid offset and sensitivity drifts with temperature. The sensors were calibrated and operated

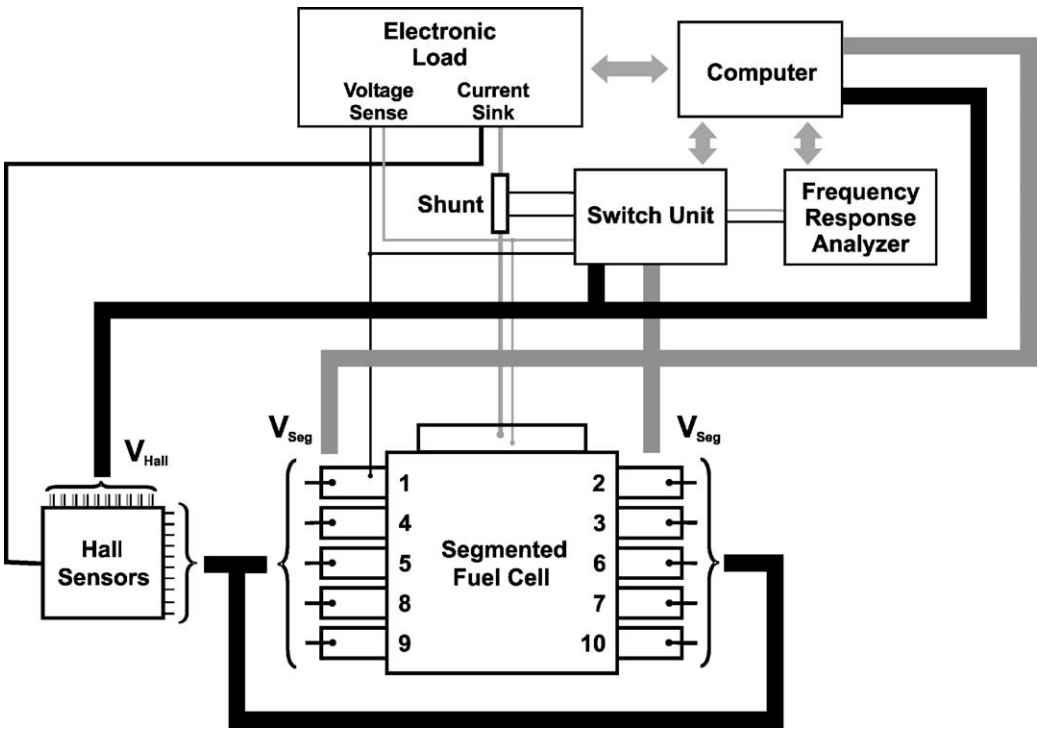

Fig. 2. Schematic of segmented cell measurement setup.

at a temperature of 50 °C. All lead wires were low gauge and kept as short as possible to keep ohmic losses to a minimum. A high amount of noise in the signal line, due to the low output impedance of the Hall sensor device, forced a decoupling of the Hall signals at the transition to the signal lines within the temperature chamber. Voltage followers individually amplified the signals for the ac impedance measurement of the high frequency resistance and for the segment current measurement. The output signals, well shielded and terminated close to the receivers, showed an average noise level less than 1 mV, equivalent to a current of $\leq$3.25 mA/cm^2. An additional set of wires sensed the segment voltages between the cathode and each anode segment, creating a four-wire measurement system to avoid offsets caused by contact resistance. A computer-controlled electronic load (Hewlett Packard, Model 6050) regulated either the total cell current or the cell voltage, by referencing to one segment voltage.

A shunt resistor in combination with a frequency response analyser (FRA) (Solartron, Model 1260) was used to measure the high frequency resistance of the total cell during operation. The FRA applied a perturbation signal to the external program input of the electronic load. Although operated in current mode, the amplitude was carefully chosen to result in a voltage perturbation smaller than 10 mV peak to peak, to keep the disturbance of the electrochemical system to a minimum. The perturbation was accompanied by a negative dc bias of half the signal size to prevent the cell from being reversed at any operation point. To increase the signal-to-noise ratio, low noise preamplifiers (SR560, Stanford Research Systems) filtered and amplified the signals before they were analysed by the FRA [4]. A Switch/Control Unit (HP 3488A) allowed selective measurement of the HFR of individual segments. Multiplexing with this device made the observation of all the individual HFRs possible during operation. But the mechanical switching from segment to segment and the measurement itself was time consuming. Measurement of all segment HFRs required a minimum of 1 min. Consequently, the HFRs of fast processes, such as CO transient measurements with high CO partial pressures (100 ppm) could not be recorded. To establish a comparison between cells of different sizes, the cell resistance was multiplied by its active area. Hence, all HFRs are given in the comparable unit, $R_{\square}$ [Ω cm^2].

The voltage and current response of the system determined the complex resistance of the fuel cell at the given operation point. The measured real part of this resistance consisted of contact resistances within the hardware, the electronic and protonic resistance of the catalyst layer, and the membrane resistance.

2.2. Sample preparation

All membrane electrode assemblies (MEAs) were prepared using the thin-film technique developed in our laboratory [5–7]. The catalyst layers were cast from inks onto a 'decal' sized in the dimensions of the desired active area. Standard ink compositions contained 5% Nafion solution (1100 equivalent wt.), 20% platinum on carbon (Vulcan XC-72, ETEK), tetrabutylammonium hydroxide, and a number of different solvents. The oven-dried ink on the decal was hot-pressed onto a Nafion polymer electrolyte membrane (N1135 or N117, in sodium form) at 210 °C, to form the membrane electrode assembly. The MEA was boiled in 0.5 mol sulphuric acid to exchange sodium and TBA^+ ions for protons, rinsed in water, and dried on a vacuum hot plate at 60 °C. Anode and cathode catalyst layers were prepared with platinum loadings of 0.2 mg Pt/cm^2.

Every electrode segment had its own decal, with an individual ink casting, drying and weighing process. For hot pressing, the decals were placed in a 'decal-frame' aligning the single active areas with the anode segments.

Unless otherwise stated, the cell was operated under the following standard conditions. The temperature of the humidifiers for the anode and the cathode were set at 105 and 80 °C, respectively. The gas humidification levels were below 100% saturation, especially at high gas flow rates as a result of limited residence time in the humidifier [1]. The operating temperature of the cell was 80 °C. Back pressure for both the anode and the cathode was 30 psig. Gas flows were controlled by electronic mass flow controllers (MKS, RS 485) calibrated with a digital flow meter (Fisher Scientific, Model 650), adjusted for the ambient pressure and temperature. The hydrogen gas flow was set to 1570 sccm equivalent to a stoichiometric flow of 1.1 if the cell was operated with a reformate gas containing 40% hydrogen and a cell current of 85 A. The cathode was typically operated on air with a fixed flow rate of 3570 sccm, equivalent to a stoichiometry of 2.5 at the same operation point.

The fuel cell was assembled with a 250 μm thick silicone coated fabric gasket on the anode and a 125 μm Teflon coated fibreglass gasket on the cathode. Double-sided (standard un-catalysed) and single-sided ETEK ELAT (V 2.22) backings were used on the anode and the cathode, respectively. The cell was assembled with a standard torque of 14.1 Nm per bolt. To assure a flat surface of the flow-field, measurements were carried out with pressure sensitive foils (pressure measuring film, Fuji Prescale Film, two-sheet type for low (25–100 bar), super low (5–25 bar), and ultra super low pressure (2–6 bar)). Variations in foil colour indicated the approximate amount of pressure applied and were used to determine continuity.

Since processes on anode and cathode are difficult to differentiate from each other, similar flow-fields on both electrodes have to be employed for the investigation of downstream effects in the fuel cell. For most of the measurements presented in this paper, identical flow-field designs for anode and cathode were employed. Six channel serpentine flow-fields were typically used to provide fuel and oxidant to the electrodes.

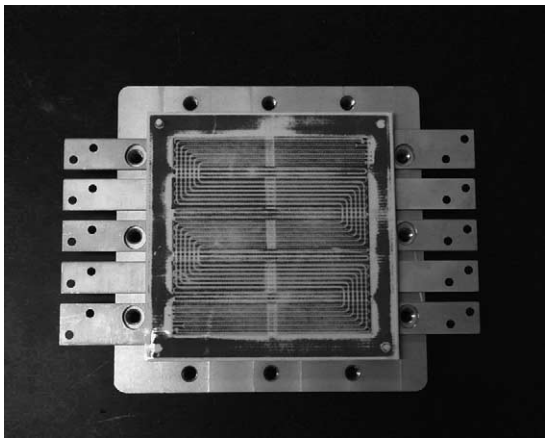

Fig. 3. Pressure test with pressure sensitive foil (super low) demonstrating homogenous pressure distribution of the segmented cell setup, when assembled with backings and gaskets. The pressure on the flow-fields varies depending on the pattern of the the flow-field alignment of the anode and cathode.

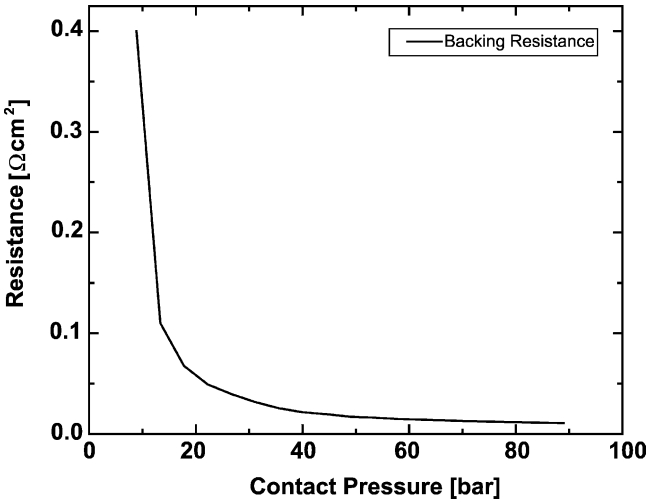

Fig. 5. Resistance of two gas diffusion backings, compressed onto each other, as a function of contact pressure. The resistance drops strongly in the beginning, then it levels out asymptotically.

3. Results and discussion

3.1. Evaluation of the segmented cell and measurement capability

3.1.1. Uniformity of flow-field surface

Fuel cells need gaskets for sealing and gas diffusion backings to establish gas transport and water management. The gaskets and backings significantly affect the pressure distribution in the hardware. Surface irregularities of the flow-field can have a large influence on the spatial contact resistance and local performance. To determine the pressure distribution in the assembled cell, a pressure measuring film was substituted for the MEA. The results are shown in Fig. 3. The highest pressures occurred in the sealing and gasket areas of the cell. These areas showed the darkest colouring on the pressure sensitive foil, due to the relatively incompressible gasket material that encircled the area of the flow-field. The lighter coloured flow-field area showed two different levels of compression. The first two segments, the middle segments and the bottom segments showed less compression than the other four segments. This variation was caused by differences in the alignment of the six channel serpentine anode with the single channel serpentine cathode flow-field. Where anode and cathode flow-fields were aligned, as shown on the left-hand side of Fig. 4, the pressure on the surface was about 70 bar. Where the flow-fields were misaligned, as indicated on the right-hand side of the figure, the pressure on the channel ridges was only about 35 bar.

The different alignments of the cell resulting in different applied pressures can have an influence on the contact resistances of the segments. For example, Fig. 5 shows the resistance change of two standard 5 cm^2 backings (ETEK ELAT single and double sided) with contact pressure, measured in a fuel cell hardware that was assembled without

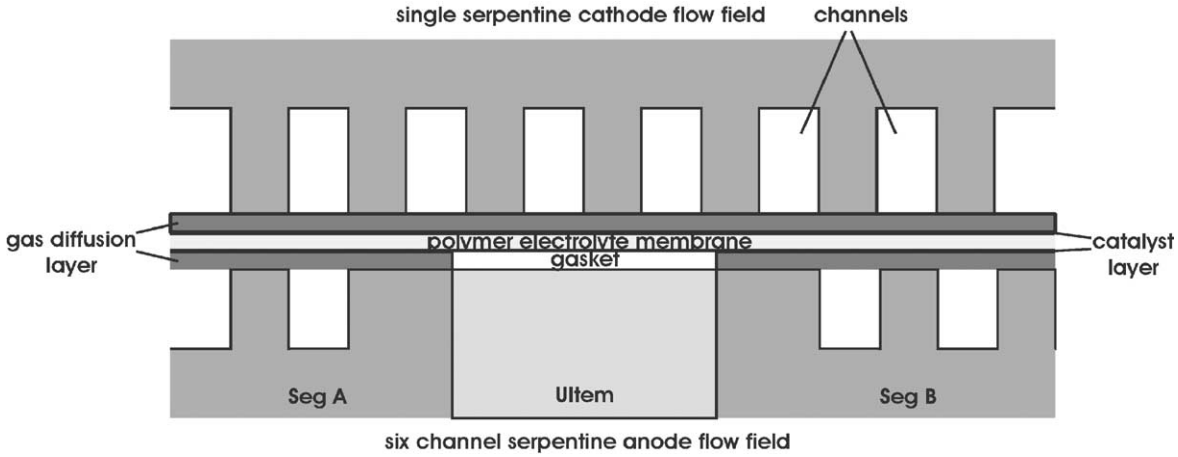

Fig. 4. Cross-section of segmented cell operated with single channel serpentine cathode flow-field, cathode backing, segmented MEA, segmented anode backing, anode gasket, and segmented six channel anode flow-field.

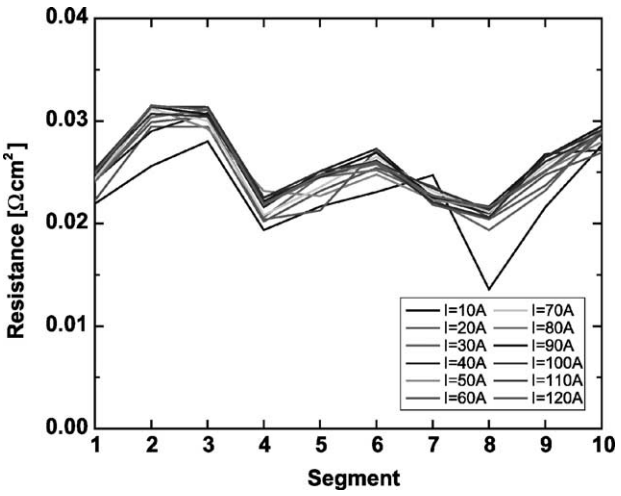

Fig. 6. The dc resistance of backings and gaskets only. The resistance alternates between two values resulting from different flow-field alignment or thickness variations of the flow-field. The resistance is about three times higher than that of a fuel cell, due to the lack of the MEA.

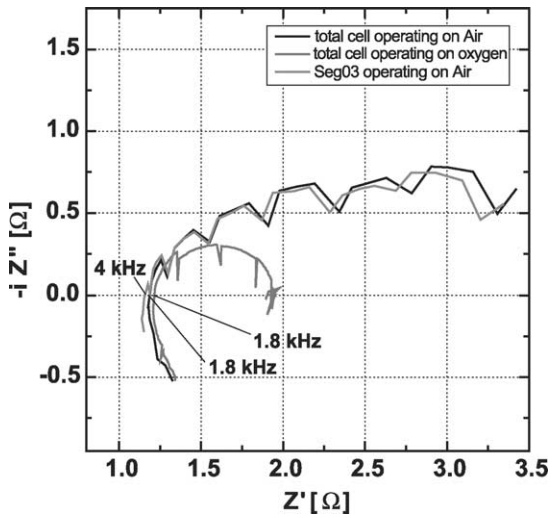

Fig. 7. Nyquist plot of ac impedance spectra of the segmented cell measured during different operating conditions. The plotted data of the total cell and segment Seg03 is uncorrected for the employed voltage and current gains.

gaskets or MEA. The resistance dropped strongly with increasing pressure applied to the fuel cell hardware, before it asymptotically levelled off to a minimum value. For contact pressures between 35 and 70 bar the relative resistance drop appeared small, but the actual change from $R_{\square} = 0.0255\,\Omega\,\mathrm{cm}^2$ (35 bar) to $R_{\square} = 0.0125\,\Omega\,\mathrm{cm}^2$ (70 bar) was significant. Consequently, if contact pressure was the main influence factor for contact resistance, we would expect alternation of the resistance value from Seg01 and Seg02 to Seg03 and Seg04 to Seg05 and Seg06, etc. due to the alignment pattern of the anode and the cathode flow-field. Measuring the dc contact resistances of the segmented cell allowed evaluation of the spatial differences of the contact pressures given by possible non-uniformities of the flow-field surface and flow-field misalignments.

Four-wire dc resistance measurements at various cell currents were carried out with the segmented cell hardware, which was assembled with backings and gaskets only. Fig. 6 shows that the resistance distribution had no common pattern with flow-field alignment. The observed resistance values of the segments range within $R_{\square} = 0.02$–$0.03\,\Omega\,\mathrm{cm}^2$, about the value observed with the $5\,\mathrm{cm}^2$ reference measurement at 35 bar compression. These values were about four to six times lower than the standard N1135 MEA resistance of $R_{\square} = 0.120\,\Omega\,\mathrm{cm}^2$, which additionally includes catalyst layer, membrane, and interface resistances. Therefore, there was a minimal contribution to contact resistance due to pressure differences between anode segments.

3.1.2. High frequency resistance measurements

Fig. 7 shows the Nyquist plots for the ac impedance of the segmented cell for air and pure oxygen over a frequency range of 1 Hz to 10 kHz. These datasets are collected with the total cell Hall sensor. The third dataset shows the ac impedance response of segment, Seg03, which is representative of all individual segments. All datasets are uncorrected for the voltage gain (20×) and current gain (1×) that was employed with the preamplifiers mentioned above. The noise associated with the measurement originated in the bandpass settings of the preamplifiers. For the following no bandpass was employed in an effort to eliminate these irregularities. The zero-crossing frequency for the total cell and the individual segment measurement were 1.8 and 4.0 kHz, respectively. This result indicates that there is an additional inductive component associated with the individual segment impedances, all of which contribute to the overall total cell impedance.

A fit of the impedance results in an equivalent circuit is shown in Fig. 8. This circuit originates from the transfer function of the measured current to the Hall sensor output voltage and the contribution of the system wires. The measured error increased with increasing frequencies from 1 Hz to 20 kHz, and although it stayed well within the specifications of the Hall sensor manufacturer of ±1 db at 60 kHz, the magnitude and phase deviations could not be ignored for ac impedance spectroscopy measurements.

Wiring passes, amplifier gain settings, fans, Hall sensors, switch boxes and other test equipment can influence the response of the cell. Thus, immediate calibration before the

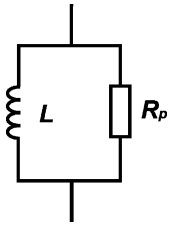

Fig. 8. Equivalent circuit of Hall sensor setup.

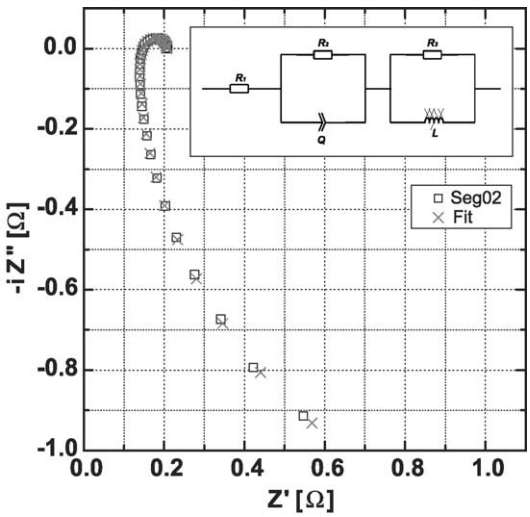

Fig. 9. The ac impedance response of the hall sensor measurement setup of Seg02 and corresponding equivalent circuit fit.

measurement ensures the best results. As an example, a test measurement on the equipment used to test Seg02, but without the cell connected, is shown in Fig. 9. The results had to be fitted to a slightly different equivalent circuit than used above. In addition to the inductive element that could be detected with the first impedance measurements a capacitive element was also found to be contributing to the system response. This element was apparently hidden within the frequency response of the fuel cell. Measurements and fits were carried out for each individual Hall sensor and for the total cell using "Equivalent Circuit" by Bernard Boukamp. The values obtained are listed in Table 1. The impedance response of the setup was subtracted from the segmented cell impedance data to obtain accurate ac impedance spectra.

To determine accurate HFRs with this setup, it was necessary to either fit and subtract the equivalent electrical circuit from the impedance data, or to adjust frequency and amplitude of the employed perturbation to create an in situ measurement of the real part of the complex resistance, i.e. an HFR measurement with phase angles of the complex resistance smaller than 5°. The resulting HFRs using either method coincided and were interchangeable. The first method was used to collect ac impedance data over the complete frequency range. The second method was chosen to measure the HFRs of the operating segmented cell to keep the measurements simple and time effective. Typically a frequency of 2 kHz was chosen for total cell measurements and 5 kHz for single segment measurements.

3.1.3. Voltage sense position

To demonstrate that the voltage sense position had no effect on determining the current distribution, measurements of the total cell voltage, current and resistance characteristics were carried out by moving the voltage sense to different segments. Fig. 10 demonstrates reproducibility of polarization curves and HFR of the total cell for voltage sense position at segments Seg01, Seg03, Seg06, and Seg10. The individual current lead wires were joined physically after measurement of the current with the Hall sensor devices, with no differences due to voltage sense position. In each of the following experiments discussed, the voltage of the anode was sensed at segment Seg01, the segment closest to the gas inlet.

3.1.4. Baseline for data interpretation

Each segment of the cell was manufactured following the same procedure to achieve similar performance under similar operating conditions. To verify this desired result the cell was operated under standard test conditions, but with only one segment connected at a time. The pressure drop at the anode was measured as 0.015 psi per segment at the given humidified hydrogen flow, the pressure drop at the cathode was 0.05 psi per segment. Taking the pressure dependence of the anode and cathode reaction into account, both values were considered negligible and the pressures along the flow-fields regarded as constant. Fig. 11 shows polarization curves of the individually operated segments measured after operating the cell at 0.5 V for 30 min. The performances and HFRs of the single segments were nearly identical confirming the reproducibility of the MEA fabrication process. The

Table 1
Fitted results of the impedance response of the measurement setup

	$R1$ [Ω]	$R2$ [Ω]	Q	n	$R3$ [Ω]	L [H]	$\sqrt{\chi}$
Total	1.36E−2	6.76E−3	1.23E−1	1.0E+0	4.86E−1	1.00E−6	2.82E−4
Cell							
Seg01	1.30E−l	7.10E−2	1.90E−2	9.35E−1	9.44E+0	8.92E−6	1.09E−4
Seg02	1.37E−1	7.00E−2	1.27E−2	1.0E+0	2.45E+0	9.01E−6	1.29E−4
Seg03	1.40E−l	5.88E−2	1.26E−2	1.0E+0	5.64E+0	1.21E−5	1.08E−4
Seg04	1.38E−l	6.49E−2	1.48E−2	9.99E−1	2.47E+0	1.01E−5	1.50E−4
Seg05	1.39E−1	5.86E−2	1.51E−2	1.0E+0	2.45E+0	8.77E−6	3.28E−4
Seg06	1.28E−1	8.27E−2	1.18E−2	9.87E−1	2.57E+0	1.01E−5	1.23E−4
Seg07	1.25E−1	7.71E−2	1.17E−2	9.93E−1	2.84E+0	1.00E−5	3.18E−4
Seg08	1.41E−1	6.37E−2	1.45E−2	1.0E+0	2.56E+0	1.28E−5	7.75E−4
Seg09	1.39E−1	5.86E−2	1.33E−2	1.0E+0	1.82E+0	1.07E−5	1.2E−3
Seg10	1.22E−1	8.37E−2	1.03E−2	9.98E−1	1.83E+0	7.79E−6	3.58E−4

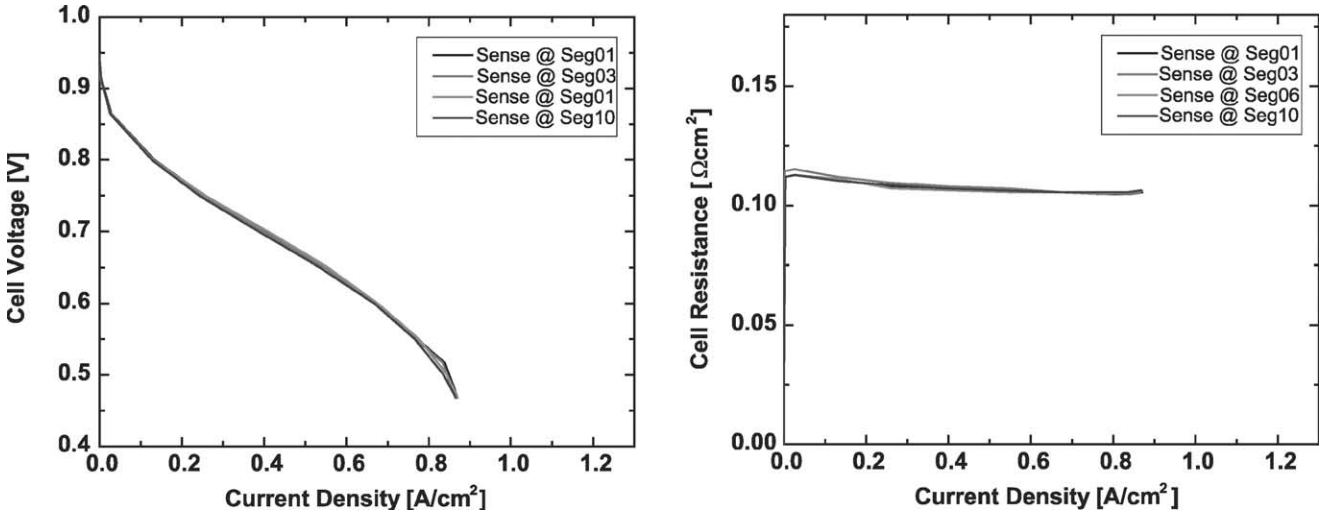

Fig. 10. Polarization curves and HFR measurements using different voltage sense positions.

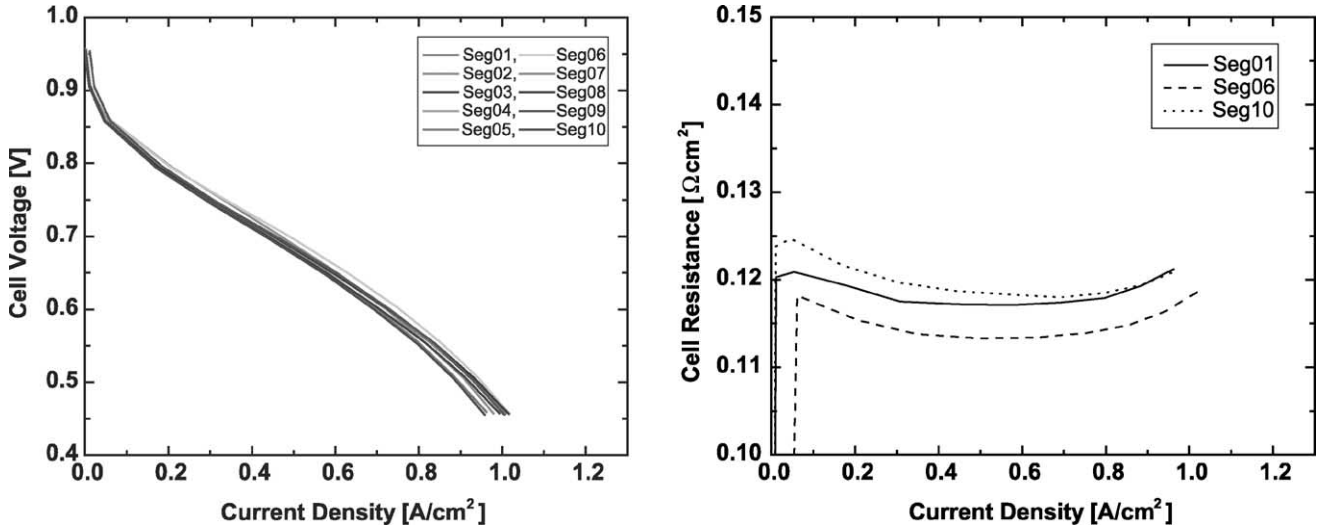

Fig. 11. Polarization curves and HFRs of cell segments operated individually at identical operation conditions. While one segment is operating, the other segments are disconnected.

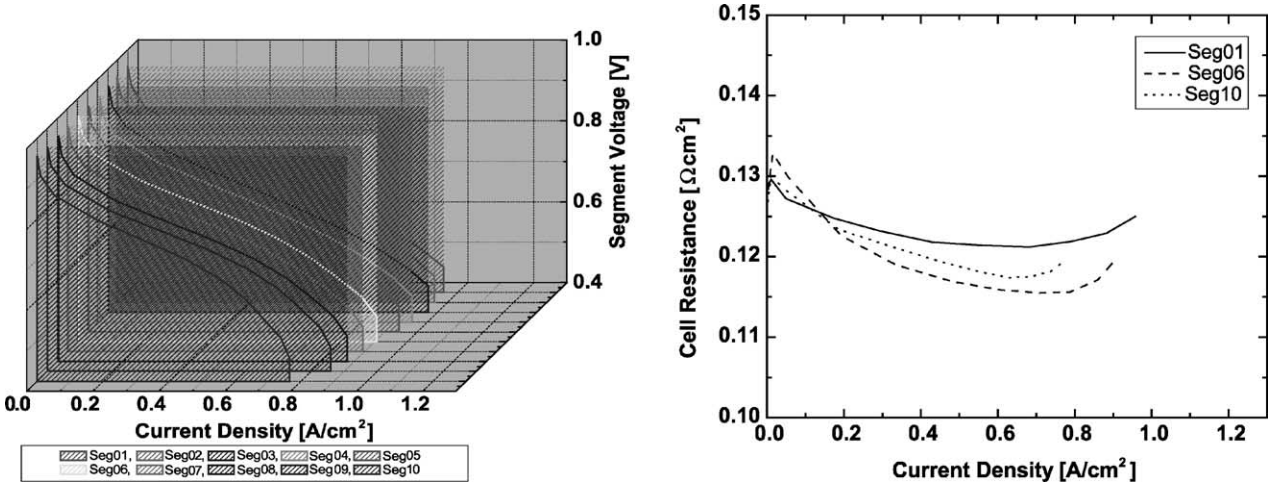

Fig. 12. Waterfall graph of the segmented cell showing the current distribution along the flow-field (left). HFRs of the segmented cell recorded during measurement of the polarization curves (right).

HFR values are close to $R_{\square} = 0.120\,\Omega\,\mathrm{cm}^2$. This is a typical HFR value for well-humidified Nafion N1135 MEAs. The pressure differences across the surface of the cell hardware measured earlier with the rigid pressure sensitive film were apparently mitigated to some extent by the use of the more pliable hydrated polymer membrane.

3.1.5. Full cell operation

Fig. 12 shows the performance characteristics of each segment of the segmented cell when all segments are in operation. The left part of Fig. 12 shows the current distributions of the segments beginning with Seg01 at the rear of the plot and moving forward sequentially. The polarization curves are different for each segment, because the operating conditions vary along the flow-field. This effect is especially notable in the high current density region of the cell where the performance decreased with each successive downstream segment. This was caused by increasing mass transport limitations along the flow channel due to the decreased concentration of oxygen and increased concentration of water in the flow stream, resulting from the upstream electrode reactions.

During cell operation, HFRs were also recorded for every segment and operating point. The HFR values for Seg01, Seg06, and Seg10 are shown in the right part of Fig. 12. The HFR of the segments was higher in the kinetic region of the polarization curves. Since the cell was operated with very high gas flows, the gas saturation level with water was less than 100% and the cell operated under somewhat dry conditions. At intermediate current densities, between 300 and 800 mA, internal hydration resulting from electrode reactions compensated for the lack of external humidification caused the HFR to decrease to about $R_{\square} = 0.120\,\Omega\,\mathrm{cm}^2$, the expected value. At high current densities, above 800 mA, the HFRs of the segments increased again, probably due to an increasing water drag through the membrane causing the anode catalyst layer to dry out slightly. Note that Seg01 showed the highest stability of the HFRs. In the kinetic region Seg01 had an HFR of $R_{\square} = 0.127\,\Omega\,\mathrm{cm}^2$ that

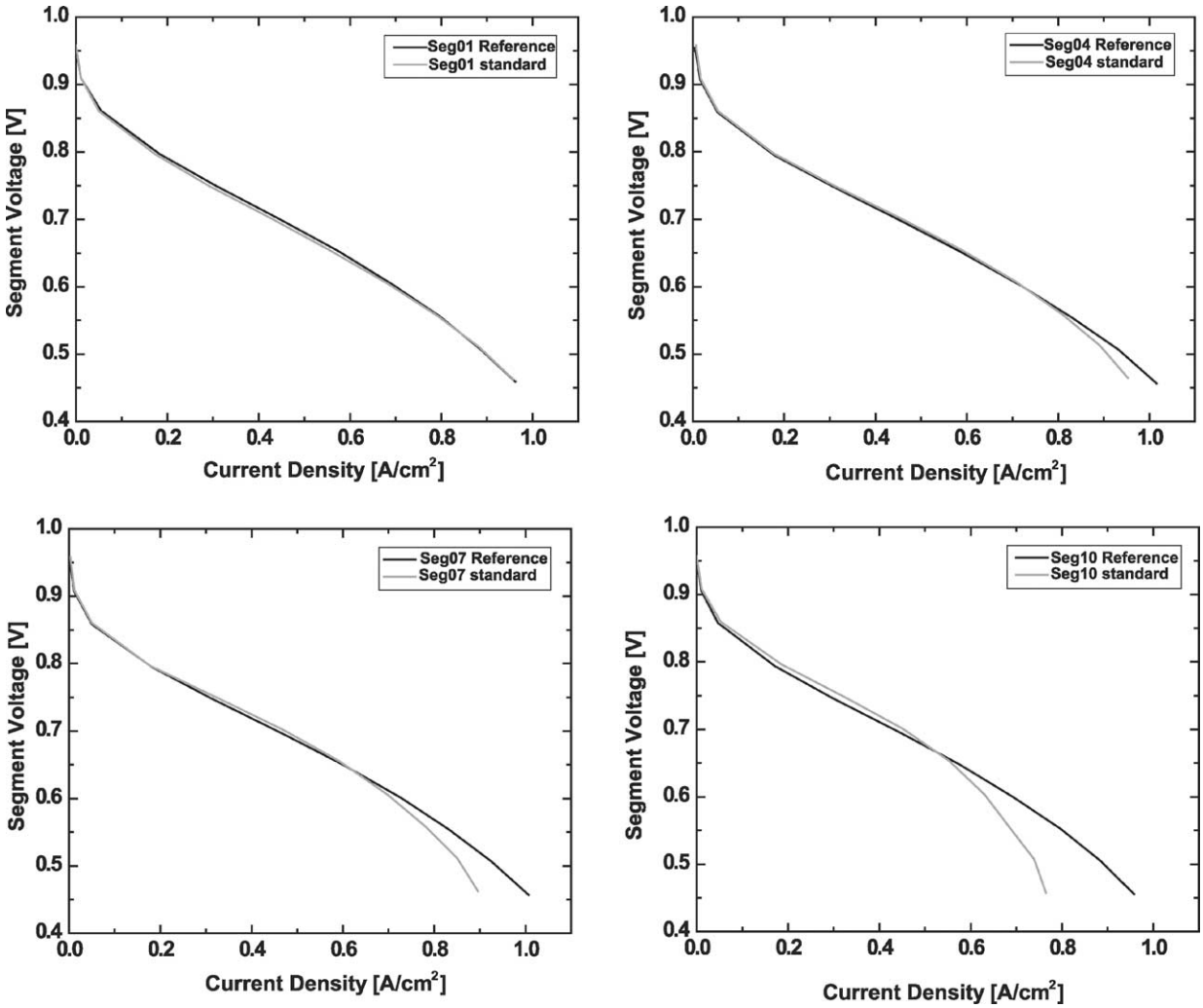

Fig. 13. Comparison of reference measurements (only one segment operating) with standard operation measurements (all segments operating) for segments Seg01, Seg04, Sego7, and Seg10.

decreased to $R_{\square} = 0.121\,\Omega\,cm^2$, and at high currents finally increased again to $R_{\square} = 0.125\,\Omega\,cm^2$. The segment was exposed to the most constant level of gas humidification due to its position closest to the gas inlet of the fuel cell hardware.

Hence, the resistance only changed with the production of reaction water within its own active area. The subsequent segments, e.g. Seg06, present larger HFR changes. The HFR of Seg06 decreased from a higher resistance of $R_{\square} = 0.133\,\Omega\,cm^2$ to a smaller resistance of $R_{\square} = 0.116\,\Omega\,cm^2$ due to the production of reaction water in the upstream segments. The increase of the HFR to $R_{\square} = 0.120\,\Omega\,cm^2$ at high current densities was identical to the increase of the inlet segment Seg01, indicating that the anode is insufficiently humidified at high current densities.

Fig. 13 shows the comparison of segments Seg01, Seg04, Seg07, and Seg10 to their baseline curves. While segment Seg01 shows no changes with respect to the reference curve, the segments further downstream deviated from their baseline performance. At small current densities, the segments benefited from the reaction water produced upstream. Their performance increased up to a specific current density, which depended on the segment position. At higher current densities the segments started to pay a performance penalty. The more segments preceding a given segment, the higher the penalty due to fuel utilisation and mass transport limitations.

4. Summary

The segmented cell hardware and procedures described herein represent a significant improvement over previous segmented cell systems. Hardware issues such as contact resistance, integrity of materials and sealing were addressed and improved. Careful evaluation of the measurement setup has led to the development of an effective investigative tool for spatial fuel cell measurements. This generation of the segmented cell was simplified to single cell operation, while at the same time the data acquisition capability was resolved into accurate distribution measurements. The new design improved the measurement accuracy, and shortened the time to measure a complete dataset by an order of magnitude. It also widened the measurement capabilities of the typical fuel cell parameters such as voltage, current, and high frequency resistance. Possible influences of the measurement setup on the measured data were minimised by referencing to the response of a single cell operating under standard conditions. Similar base-lining of ac impedance measurements was made by determining the contribution of the experimental setup to the measured cell response.

This paper demonstrates how the segmented cell approach can be used as a diagnostic tool to measure downstream effects in operating fuel cells. Even under carefully controlled, normal operating conditions, the effect of water management on downstream segments was observed and quantified. The segmented cell approach will be used to study the anode CO poisoning process, flow-field design effects and humidification issues, which will be the topics of future publications.

Acknowledgements

This work was conducted at LANL for the Department of Energy under Prime Contract W-7405-ENG-36. Support by the DOE Office of Hydrogen, Fuel Cells and Infrastructure Technologies is gratefully acknowledged. G.B would also like to thank Dr. Wayne Smith and Prof. Dr. U. Stimming from the Technical University of Munich for their encouragement and support. We gratefully acknowledge Dr. T.E. Springer for fruitful discussions regarding ac impedance spectroscopy.

References

[1] S. Cleghorn, C.R. Derouin, M.S. Wilson, S. Gottesfeld, J. Appl. Electrochem. 28 (1998) 663–672.
[2] Ch. Wieser, A. Helmbold, E. Gtilzow, J. Appl. Electrochem. 30 (2000) 803–807.
[3] J. Stumper, S.A. Campbell, D.P. Wilkinson, M.C. Johnson, M. Davis, Electrochim. Acta 43 (24) (1998) 3773–3783.
[4] T. Springer, M. Wilson, S. Gottesfeld, J. Electrochem. Soc. 140 (1993) 3513.
[5] M.S. Wilson, S. Gottesfeld, J. Appl. Electrochem. 22 (1992) 1.
[6] M.S. Wilson, S. Gottesfeld, J. Electrochem. Soc. 139 (1992) L28.
[7] M.S. Wilson, J.A. Valerio, S. Gottesfeld, Electrochim. Acta 40 (1995) 355–363.